

# The nearby population of M dwarfs with WISE: A search for warm circumstellar dust

Henning Avenhaus, Hans Martin Schmid, and Michael R. Meyer

Institute for Astronomy, ETH Zurich, Wolfgang-Pauli-Strasse 27, CH-8093 Zurich, Switzerland

Received 11 June 2012 / Accepted 30 August 2012

## ABSTRACT

**Context.** Circumstellar debris disks are important because of their connection and interaction with planetary systems. An efficient way to identify such systems is through their infrared excess. Most studies so far concentrated on early-type or solar-type stars, but less effort has gone into M dwarfs, which have the additional problem that the mid-infrared colors are poorly known.

**Aims.** We characterize the infrared photometric behavior of M dwarfs and search for infrared excess in nearby M dwarfs taken from the volume-limited RECONS sample, concentrating on mid-infrared wavelengths corresponding to warm ( $\gtrsim 100$  K) dust. We then check whether the population of these late-type stars has a significantly different fraction of infrared excess compared to earlier-type stars.

**Methods.** We use data recently released from the *WISE* satellite which provides the most sensitive mid-infrared all-sky survey to date. Our sample consists of 85 sources encompassing 103 M dwarfs. We compare this sample to *Spitzer* data and match it to the 2MASS catalog. We derive empirical infrared colors from these data and discuss the intrinsic spread within these colors as well as the errors from *WISE* and 2MASS. From this, we check the stars for infrared excess and discuss the minimum excess we would be able to detect.

**Results.** Other than the M8.5 dwarf SCR 1845-6357 A, where the mid-infrared excess is produced by a known T6 companion, we detect no excesses in any of our sample stars. The limits we derive for the  $22\mu\text{m}$  excess are slightly larger than the usual detection limit of  $\sim 10$ -15% for *Spitzer* studies, but the inclusion of the  $12\mu\text{m}$  band and the  $[12] - [22]$  color in our analysis allows us to put tight constraints on the fractional dust luminosity  $L_{\text{dust}}/L_{\star}$ . Comparing to earlier-type stars, we show that this result is not inconsistent with M dwarf excesses in the mid-infrared being as frequent as excesses around earlier-type stars. The low detection rate of  $0^{+1.3}_{-0.0}\%$  we derive for our sample in that case is an age effect. We also present a tentative excess detection at  $22\mu\text{m}$  around the known cold debris disk M dwarf AU Mic, which is not part of our statistical sample.

**Conclusions.** There is still no clear detection of a mid-infrared excess around any old ( $\gtrsim 30$  Myr) main-sequence M dwarf. It is unclear whether this is due to a different dust evolution around M dwarfs compared to earlier-type stars or whether this is an age effect combined with the difficulties involved in searching M dwarfs for infrared excesses. A significantly larger sample of well-studied M dwarfs will be required to solve this question. At the same time, their behavior at longer wavelengths which are sensitive to colder dust needs further investigation.

**Key words.** Stars: circumstellar matter - Stars: late-type - Stars: individual: AU Mic - Infrared: stars - Methods: observational - Methods: statistical

## 1. Introduction

Dust around main-sequence stellar systems has become a very well-studied phenomenon since it was first seen. The first detection was made around Vega, an A0 star, through the detection of infrared excess (Aumann et al., 1984). A large amount of stars showing this “Vega phenomenon” was subsequently detected and imaged through the all-sky survey performed by *IRAS* at 25, 60 and  $100\mu\text{m}$  (Zuckerman, 2001; Rhee et al., 2007), as well as with pointed observations using *ISO* (Decin et al., 2003; Spangler et al., 2001) at 60 and  $100\mu\text{m}$ , *Spitzer* (Rebull et al., 2008; Carpenter et al., 2009; Koerner et al., 2010) at 24 and  $70\mu\text{m}$ , and *Herschel* (most recently by Acke et al. (2012)). Recently, the all-sky *AKARI* satellite was able to make detections at 9 and  $18\mu\text{m}$  wavelength (Fujiwara et al., 2009).

It was quickly realized that the infrared excess must stem from dust which surrounds the star in a disk. It was furthermore understood that micron-sized dust can not persist in orbit around a star for very long due to effects like radiation pressure, Poynting-Robertson drag, and stellar wind pressure. Thus, the dust has to be permanently regenerated in situ. The standard interpretation of this is that the debris traces underlying

planetesimal belts, where dust is generated through collisions (Backman & Paresce, 1993). The same effect happens in the solar system’s asteroid belt and is responsible for zodiacal light. The difference to the solar system is that these belts are mostly collisionally dominated, producing a much stronger infrared excess signal than the solar system debris disk does.

The first detection of this phenomenon was made around an A star. Because these bright stars are easiest to observe, the detection of an infrared excess is relatively easy for A, F, G and nearby K stars. Late-type star and specifically M-dwarf infrared excesses are significantly harder to detect. First, they are much fainter, and secondly, for M dwarfs the Rayleigh-Jeans approximation does not hold in the mid-infrared. Molecular bands dominate their spectra at visible and near-infrared wavelengths. Because of this, the expected scatter in their mid- and far-infrared colors is larger compared to early-type stars. Most searches for infrared excess concentrate on early-type or solar-type stars (e.g., Su et al. (2006); Bryden et al. (2009); Moór et al. (2011)).

A second effect is that the frequency of debris disks declines with age (Carpenter et al., 2009). Vega has an age of only  $\sim 450$  Myr (Yoon et al., 2010), and many studies for infrared excesses

around early-type stars include very young targets (e.g. Su et al. (2006)). Very few young main-sequence M dwarfs are known; one of them is the well-studied debris disk system AU Mic (e.g., Fitzgerald et al. (2007)). This is because of the intrinsic faintness of M dwarfs, which only allows detecting them if they are close to the solar system. M dwarf debris disk surveys are thus usually bound to target mostly old stars, where the excess frequency is expected to be lower. Of course, many TTauri stars are M dwarfs with strong mid-IR excess from primordial disk emission and there is also growing evidence that primordial disks last longer around lower-mass stars (Carpenter et al., 2006), but no mid-infrared excesses attributable to debris have been found except around AT Mic, like AU Mic a member of the  $\sim 12$  Myr  $\beta$  Pictoris moving group (Gautier et al., 2007; Plavchan et al., 2009). Few detections of cold, Kuiper belt like debris disks have been made in the sub-mm regime for young M dwarfs (Liu et al., 2004; Lestrade et al., 2009), at a seemingly lower rate than for earlier-type stars. It has been pointed out that there is an apparent lack of debris disk around older M dwarfs in general (Plavchan et al., 2005).

On the other hand, M dwarfs make up the majority of stars in our galaxy, which gives good reasons to study them. Because of its magnitude limits and the intrinsic faintness of M dwarfs, *IRAS* can only give access to the very closest M dwarf systems. The recently flown *WISE* satellite does not have the far-infrared capabilities of *IRAS*, but goes significantly deeper in the 12- and 22- $\mu$ m bands, giving access to more M dwarf systems (Wright et al., 2010). M dwarf studies going this deep have been possible earlier only with dedicated pointed observations, for example using the *Spitzer* space telescope (Werner et al., 2004).

Theoretical studies of the behavior and evolution of dust around M dwarfs suggest that the timescales and frequencies involved in M dwarfs might be considerably different from what we observe in earlier-type stars (Plavchan et al., 2005). Observationally, there is a lack of solid evidence for a difference in either the frequency or the timescales to disperse debris discs when comparing M dwarfs to earlier-type stars. No studies were able to prove a statistically significant difference between A-stars and solar-type stars, either (Trilling et al., 2008). The question whether the processes involved in the evolution of debris disks work similar over a wide range of stellar luminosities or whether there are significant differences is so far unresolved.

We describe the data we acquired from *WISE* and 2MASS in section 2. In section 3, we describe the analysis of the data, our efforts to detect mid-infrared excesses and the limits we can derive from this on the excess at different wavelengths and on the dust surrounding the M dwarfs in our sample. In section 4, we compare our study to other results from both other M dwarf surveys as well as surveys of earlier-type stars. We discuss implications in section 5 and draw our conclusions in section 6.

## 2. Source Data from RECONS, WISE, and 2MASS

The *WISE* satellite was launched on December 14, 2009 and began its operations in January 2010, scanning the complete sky in four wavebands centered at 3.4, 4.6, 12 and 22  $\mu$ m, named w1 through w4 (Wright et al., 2010). On April 14, 2011, a preliminary data release covered about 57 percent of the sky. On March 14, 2012, the all-sky catalogue was released. The *WISE* satellite is significantly more sensitive than the *IRAS* satellite was, and is also more sensitive than the more recent *AKARI* sky survey (Murakami et al., 2007). Its 5- $\sigma$  detection limits are 16.4, 15.4, 11.1 and 7.8 magnitudes, respectively. The *WISE* beams have

FWHM of 6.1'', 6.4'', 6.5'' and 12'', respectively. This means that close binary systems can not be resolved, an aspect we will have to take into account.

The 2MASS survey covered the entire sky in the *J*, *H* and *K<sub>s</sub>* wavebands during the years 1997 through 2001 using ground-based facilities (Skrutskie et al., 2006). Both its sensitivity as well as its resolution are better than the *WISE* limits. The errors in the 2MASS magnitudes stem mainly from atmospheric effects and calibration uncertainties.

### 2.1. Stellar sample

Because of the intrinsic faintness of late-type dwarfs, and because of the magnitude limit of *WISE*, which is still relatively strict at 7.8 magnitudes in the longest wave band, a study of the mid-infrared behavior and excesses has to focus on nearby M dwarfs. Very late M dwarfs (M7, M8, M9) are too faint for the *WISE* 22  $\mu$ m band even at distances of only 10 pc, while early-type M dwarfs (M0, M1) can be usefully tracked out to distances of 25 pc or more. Because our aim is to have a sample not biased heavily towards early-type M dwarfs, and because M8 and M9 dwarfs are intrinsically more rare than M0 and M1 dwarfs (the IMF peaks around M3-M4 (Bastian et al., 2010)), we concentrate on the immediate solar neighborhood, omitting a lot of early-type M dwarfs that would be within reach of *WISE*, but are beyond 10pc.

One of the best and most complete samples of the immediate solar vicinity is the list of the 100 nearest stellar systems by the RECONS team (Jao et al., 2005; Henry et al., 2006). Including eight systems that were pushed out of the top 100 list, it consists of 108 systems encompassing 139 stars (not counting planets and white or brown dwarfs, which also appear in the catalog). The vast majority of these stars are M dwarfs (110). One of the advantages of the RECONS sample is that besides giving accurate positions and proper motions (required because these very near objects move significantly on sky between the 2MASS and *WISE* surveys), it also gives accurate parallaxes, which can be used to determine absolute luminosities. V magnitudes are also provided. RECONS can thus give a clean, very complete volume limited sample, which is ideal for our purpose. It was also readily available at the time we started our analysis, in contrast to, for example, the Reid 8pc sample (Reid et al., 2007), which would have been another option. The number of M dwarfs in the Reid sample is slightly larger. However, the statistical analysis we want to perform can be done equally well with the RECONS sample, and the slightly larger number of M dwarfs in the Reid sample would not significantly change our discussion.

### 2.2. Observational data

All M dwarfs in the RECONS sample can be visually seen at the expected positions in the *WISE* images. Because some of the stars are confused with nearby earlier stars and/or tight binary M dwarf companions, there are however only 90 individual sources for the 110 M dwarfs in the catalogue. Out of these, five sources containing seven stars (GJ 783 B, GJ 338 A, LP 771-095 A/B/C, GJ 725 A and GJ 725 B) had to be removed from our analysis due to bad data quality, mostly from confusion with nearby sources. One more star (GJ 752 B) had to be excluded from the analysis of the 22  $\mu$ m band because it could not be detected at this wavelength. A summary of the excluded sources and the reasons for exclusion is presented in Table 1. This leaves 103 M dwarfs in 85 individual *WISE* sources (70 single, 12 double and

Table 2. Observational data

Name	stars in beam	Distance (pc) <sup>a</sup>	Spectral Type <sup>b</sup>	V (mag) <sup>c</sup>	K <sub>s</sub> (mag) <sup>d</sup>	F <sub>3,4</sub> (mag) <sup>e</sup>	F <sub>12</sub> (mag) <sup>e</sup>	F <sub>22</sub> (mag) <sup>e</sup>
GJ 551	1	1.30±0.01	M5.5	11.05	4.38±0.03	4.20±0.09	3.83±0.02	3.66±0.02 <sup>j</sup>
GJ 699	1	1.83±0.01	M4.0	9.57	4.52±0.02	4.39±0.07	4.04±0.02	3.92±0.03 <sup>j</sup>
GJ 406	1	2.39±0.01	M6.0	13.53	6.08±0.02	5.81±0.06	5.48±0.02	5.31±0.03 <sup>j</sup>
GJ 411	1	2.54±0.01	M2.0	7.47	3.25±0.31	3.24±0.14	3.05±0.01	2.93±0.02 <sup>j</sup>
GJ 65 A/B	2	2.68±0.02	M5.5 / M6.0	12.06	5.34±0.02	5.05±0.07	4.76±0.02	4.62±0.03
GJ 729	1	2.97±0.02	M4.0	10.44	5.37±0.02	5.16±0.06	4.91±0.01	4.72±0.03 <sup>j</sup>
GJ 905	1	3.16±0.01	M5.0	12.29	5.93±0.02	5.69±0.06	5.39±0.02	5.25±0.03 <sup>j</sup>
GJ 887	1	3.28±0.01	M1.0	7.34	3.47±0.20	3.24±0.12	3.08±0.01	3.00±0.02 <sup>j</sup>
GJ 447	1	3.35±0.02	M4.0	11.16	5.65±0.02	5.46±0.06	5.18±0.01	5.03±0.03 <sup>j</sup>
GJ 866 A/B/C	3	3.45±0.05	M5.5 / M / M	12.30	5.54±0.02	5.31±0.06	5.01±0.02	4.88±0.03
GJ 15 A	1	3.57±0.01	M2.0	8.08	4.02±0.02	3.85±0.10	3.71±0.02	3.60±0.02 <sup>j</sup>
GJ 15 B	1	3.57±0.01	M4.0	11.06	5.95±0.02	5.75±0.05	5.46±0.02	5.30±0.03 <sup>j</sup>
GJ 1111	1	3.63±0.04	M6.0	14.90	7.26±0.02	7.03±0.03	6.63±0.02	6.47±0.06 <sup>j</sup>
GJ 1061	1	3.68±0.02	M5.5	13.09	6.61±0.02	6.37±0.05	6.01±0.02	5.87±0.03 <sup>j</sup>
GJ 54.1	1	3.72±0.04	M4.0	12.10	6.42±0.02	6.17±0.04	5.89±0.01	5.72±0.04 <sup>j</sup>
GJ 273	1	3.76±0.01	M4.0	9.85	4.86±0.02	4.72±0.07	4.46±0.02	4.33±0.03 <sup>j</sup>
SCR 1845-6357 A	1	3.85±0.02	M8.5 <sup>f</sup>	17.40	8.51±0.02	8.14±0.02	7.38±0.02	7.08±0.07
SO 0253+1652	1	3.85±0.01	M6.0	15.14	7.59±0.05	7.32±0.03	6.90±0.02	6.72±0.08
GJ 191	1	3.91±0.01	M1.0	8.85	5.05±0.02	4.95±0.08	4.72±0.01	4.60±0.03 <sup>j</sup>
DEN 1048-3956	1	4.02±0.02	M8.5 <sup>f</sup>	17.39	8.45±0.02	8.10±0.02	7.46±0.02	7.23±0.09
GJ 860 A/B	2	4.03±0.02	M3.0 / M4.0	9.57	4.78±0.03	4.69±0.08	4.30±0.01	4.12±0.03
GJ 234 A/B	2	4.09±0.02	M4.0 / M	11.12	5.49±0.02	5.29±0.07	4.99±0.01	4.84±0.03
GJ 628	1	4.27±0.03	M4.0	10.10	5.08±0.02	4.91±0.07	4.67±0.01	4.57±0.03 <sup>j</sup>
GJ 1	1	4.34±0.02	M2.0	8.54	4.52±0.02	4.36±0.09	4.20±0.01	4.07±0.02 <sup>j</sup>
GJ 473 A/B	2	4.39±0.09	M5.5 / M	12.49	6.04±0.02	5.79±0.05	5.49±0.01	5.35±0.04
GJ 83.1	1	4.45±0.06	M4.0	12.31	6.65±0.02	6.44±0.04	6.10±0.01	5.96±0.04 <sup>j</sup>
GJ 687	1	4.54±0.02	M3.0	9.17	4.55±0.02	4.40±0.09	4.18±0.02	4.06±0.02 <sup>j</sup>
LHS 292	1	4.54±0.07	M6.5	15.73	7.93±0.03	7.71±0.02	7.30±0.02	7.03±0.09 <sup>j</sup>
GJ 1245 A/C	2	4.54±0.02	M5.5 / M	13.41	6.85±0.02	6.60±0.07	6.24±0.02	6.08±0.05
GJ 1245 B	1	4.54±0.02	M5.5	14.01	7.39±0.02	7.18±0.07	6.85±0.02	6.77±0.09 <sup>j</sup>
GJ 674	1	4.54±0.03	M3.0	9.37	4.86±0.02	4.71±0.08	4.50±0.02	4.34±0.03 <sup>j</sup>
GJ 876 A	1	4.66±0.01	M4.0	10.18	5.01±0.02	4.84±0.08	4.64±0.01	4.54±0.03 <sup>j</sup>
GJ 1002	1	4.69±0.08	M5.0	13.77	7.44±0.02	7.18±0.03	6.86±0.02	6.77±0.08 <sup>j</sup>
LHS 288	1	4.77±0.06	M5.0	13.92	7.73±0.03	7.50±0.03	7.09±0.02	6.75±0.07 <sup>j</sup>
GJ 412 A	1	4.86±0.02	M2.0	8.77	4.77±0.02	4.64±0.09	4.46±0.01	4.36±0.02 <sup>j</sup>
GJ 412 B	1	4.86±0.02	M5.5	14.44	7.84±0.03	7.61±0.02	7.22±0.02	7.12±0.09 <sup>j</sup>
GJ 388	1	4.89±0.07	M3.0	9.29	4.59±0.02	4.42±0.09	4.27±0.02	4.15±0.03 <sup>j</sup>
GJ 832	1	4.95±0.02	M2.0	8.66	4.50±0.02	4.29±0.08	4.16±0.01	4.05±0.02 <sup>j</sup>
LP 944-020	1	4.97±0.10	M9.0 <sup>g</sup>	18.69	9.55±0.02	9.13±0.02	8.27±0.02	8.00±0.11 <sup>j</sup>
GJ 166 C	1	4.98±0.01	M4.0	11.24	5.96±0.03	5.81±0.05	5.48±0.02	5.34±0.04 <sup>j</sup>
GJ 873	1	5.05±0.02	M3.0	10.22	5.30±0.02	5.24±0.06	4.89±0.02	4.75±0.03
GJ 682	1	5.05±0.05	M4.0	10.95	5.61±0.02	5.35±0.07	5.20±0.02	5.13±0.04 <sup>j</sup>
GJ 1116 A/B	2	5.23±0.07	M5.5 / M	13.65	6.89±0.02	6.64±0.04	6.28±0.02	6.21±0.08
G 099-049	1	5.24±0.05	M4.0	11.31	6.04±0.02	5.94±0.05	5.61±0.02	5.47±0.04
LHS 1723	1	5.32±0.04	M4.0	12.22	6.74±0.02	6.53±0.05	6.23±0.02	6.13±0.05
GJ 445	1	5.34±0.05	M3.0	10.79	5.95±0.03	5.75±0.06	5.51±0.02	5.38±0.03
GJ 526	1	5.41±0.02	M2.0	8.46	4.42±0.02	4.37±0.10	4.19±0.01	4.10±0.02
GJ 169.1 A	1	5.54±0.02	M4.0	11.04	5.72±0.02	5.54±0.06	5.32±0.01	5.20±0.03
GJ 251	1	5.61±0.05	M3.0	10.02	5.28±0.02	5.16±0.07	4.92±0.02	4.78±0.03
2MA 1835+3259	1	5.67±0.02	M8.5 <sup>f</sup>	18.27	9.17±0.02	8.80±0.02	8.16±0.02	7.89±0.13
GJ 205	1	5.68±0.03	M1.0	7.95	4.04±0.26	3.74±0.12	3.70±0.02	3.63±0.02
LP 816-060	1	5.71±0.11	M4.0	11.50	6.20±0.02	6.02±0.05	5.77±0.02	5.63±0.04
GJ 229 A	1	5.75±0.03	M1.0	8.14	4.17±0.23	4.06±0.13	3.97±0.02	3.82±0.04
GJ 213	1	5.83±0.03	M4.0	11.57	6.39±0.02	6.23±0.05	5.90±0.02	5.68±0.04
GJ 693	1	5.84±0.08	M3.0	10.76	6.02±0.02	5.92±0.06	5.60±0.02	5.48±0.04
GJ 752 A	1	5.85±0.02	M3.0	9.10	4.67±0.02	4.47±0.08	4.38±0.01	4.27±0.03
GJ 752 B	1	5.85±0.02	M7.0	17.45	8.77±0.02	8.47±0.02	8.08±0.02	N/A
GJ 570 B/C	2	5.86±0.02	M2.0 / M	8.09	3.80±0.23	4.06±0.06	3.74±0.02	3.62±0.03
GJ 754	1	5.91±0.05	M4.0	12.23	6.85±0.03	6.65±0.03	6.36±0.02	6.20±0.06
GJ 588	1	5.93±0.04	M3.0	9.31	4.76±0.02	4.70±0.07	4.46±0.01	4.36±0.03
GJ 1005 A/B	2	5.94±0.03	M4.0 / M	11.49	6.39±0.02	6.17±0.04	5.91±0.02	5.81±0.04
GJ 908	1	5.95±0.04	M1.0	8.98	5.04±0.02	5.02±0.07	4.76±0.02	4.66±0.03
GJ 285	1	5.98±0.07	M4.0	11.19	5.70±0.02	5.51±0.06	5.29±0.01	5.13±0.03
GJ 268 A/B	2	6.12±0.07	M4.0 / M	11.48	5.85±0.02	5.69±0.06	5.38±0.02	5.20±0.03

**Table 2.** Observational data (contd.)

Name	stars in beam	Distance (pc) <sup>a</sup>	Spectral Type <sup>b</sup>	V (mag) <sup>c</sup>	K <sub>s</sub> (mag) <sup>d</sup>	F <sub>3.4</sub> (mag) <sup>e</sup>	F <sub>12</sub> (mag) <sup>e</sup>	F <sub>22</sub> (mag) <sup>e</sup>
GJ 784	1	6.20±0.04	M0.0	7.95	4.28±0.02	4.15±0.10	4.05±0.02	3.98±0.02
GJ 555	1	6.22±0.08	M4.0	11.32	5.94±0.03	5.79±0.06	5.54±0.02	5.41±0.03
GJ 896 A/B	2	6.25±0.06	M3.0 / M5.0 <sup>h</sup>	10.10	4.94±0.03	4.76±0.08	4.64±0.02	4.59±0.03
GJ 581	1	6.34±0.07	M3.0	10.57	5.84±0.02	5.69±0.06	5.48±0.01	5.33±0.03
LHS 2090	1	6.37±0.11	M6.0	16.10	8.44±0.02	8.23±0.03	7.80±0.02	7.96±0.22
LHS 337	1	6.38±0.08	M4.0	12.75	7.39±0.02	7.24±0.03	6.86±0.02	6.72±0.05
GJ 661 A/B	2	6.40±0.05	M3.0 / M	9.37	4.83±0.02	4.71±0.08	4.46±0.02	4.34±0.02
G 180-060	1	6.41±0.16	M5.0	14.76	8.51±0.02	8.29±0.02	7.95±0.02	7.90±0.13
GJ 644 A/B/D	3	6.45±0.02	M3.0 / M / M	9.03	4.40±0.04	4.22±0.09	4.04±0.02	3.90±0.03
GJ 644 C	1	6.45±0.02	M6.5	16.78	8.82±0.02	8.59±0.02	8.13±0.02	7.86±0.18 <sup>j</sup>
GJ 643	1	6.45±0.02	M4.0	11.80	6.72±0.02	6.57±0.03	6.29±0.02	6.12±0.05
GJ 625	1	6.53±0.04	M2.0	10.10	5.83±0.02	5.68±0.06	5.46±0.02	5.33±0.02
GJ 1128	1	6.53±0.10	M4.0	12.74	7.04±0.02	6.80±0.03	6.51±0.01	6.40±0.03
GJ 1156	1	6.54±0.13	M5.0	13.80	7.57±0.03	7.33±0.03	6.99±0.02	6.91±0.08
LHS 3003	1	6.56±0.09	M6.5	17.05	8.93±0.03	8.69±0.02	8.27±0.02	8.12±0.27 <sup>j</sup>
GJ 408	1	6.70±0.07	M3.0	10.02	5.50±10.00	5.38±0.06	5.19±0.01	5.09±0.03
GJ 829 A/B	2	6.71±0.08	M3.0 / M	10.30	5.45±0.02	5.30±0.07	5.06±0.01	4.90±0.03
G 041-014 A/B/C	3	6.77±0.09	M5.0 / M / M <sup>i</sup>	11.46	5.69±0.02	5.49±0.06	5.25±0.02	5.08±0.03
GJ 402	1	6.80±0.14	M4.0	11.65	6.37±0.02	6.26±0.05	5.98±0.02	5.86±0.04
GJ 880	1	6.83±0.04	M2.0	8.65	4.52±0.02	4.43±0.08	4.33±0.01	4.22±0.02
GJ 299	1	6.84±0.14	M4.0	12.82	7.66±0.03	7.44±0.03	7.12±0.02	7.01±0.09

**Notes.**

- (<sup>a</sup>) Distances calculated from RECONS parallaxes (Henry et al., 2006).  
(<sup>b</sup>) Photometric spectral types are given based on the calibrations from Bessell (1991) for spectral types up to M7.5. In case of multiples, these represent the primary of the system. The secondary / tertiary spectral types are taken from the RECONS database. A 'M' spectral type means that the exact spectral type is unknown.  
(<sup>c</sup>) V magnitudes taken from the RECONS database; where more than one star is in the *WISE* / 2MASS beam, the fluxes are added up.  
(<sup>d</sup>) K<sub>s</sub> magnitudes and errors are taken from the 2MASS database (Skrutskie et al., 2006); where more than one star is in the *WISE* beam, the fluxes of all stars in the beam are added up.  
(<sup>e</sup>) *WISE* bands w1 centered at 3.4μm, w3 centered at 12μm, and w4 centered at 22μm (Wright et al., 2010).  
(<sup>f</sup>) Spectral type from Henry et al. (2004).  
(<sup>g</sup>) Spectral type from Kirkpatrick et al. (1997).  
(<sup>h</sup>) Both primary and secondary spectral types based on calibrations from Bessell (1991), because the system is resolved in 2MASS.  
(<sup>i</sup>) RECONS gives a spectral type of M3.5 for the primary.  
(<sup>j</sup>) Stars with 24 μm *Spitzer* flux measurements from Gautier et al. (2007).

**Table 1.** Excluded stars

Name	reason for exclusion
GJ 783 B	confusion with nearby (7") K2.5 primary
GJ 338 A	confusion with nearby (17") K7 secondary
LP 771-095 A/B/C	WISE catalog shows multiple sources at expected position, but none of them matches the star
GJ 725 A/B	Close binary system (14") which has very bad SNR due to mutual contamination
GJ 752 B	Excluded from analysis of w4 band, not detected in WISE w4

**Notes.** Stars that were excluded from the analysis for reasons of data quality.

3 triple systems) for our analysis (one single star less for the w4 band).

Table 2 shows the observational data for these 85 sources. The *WISE* data is complemented with K<sub>s</sub> magnitudes from the 2MASS survey and photometric spectral types as well as V band data and distance information from RECONS. If multiple stars were present in the *WISE* beam, the V magnitudes were calculated by combining the single-source V band magnitudes from

RECONS. In the single case that stars were unresolved in *WISE*, but resolved with 2MASS (GJ 896 A/B), the 2MASS magnitudes were calculated in the same way. In all other cases, the sources were confused in 2MASS as well.

For the purposes of this paper, the data from three of the four *WISE* bands is used: The first, third and fourth. The second band, centered at 4.6 μm, is omitted. The reason is that while the w4 band is just about able to pick up the faintest and farthest dwarfs in our sample at magnitudes beyond 8, the *WISE* measurements for the earlier bands run into saturation at magnitudes brighter than ~6. While the first *WISE* band behaves quite well and high-quality magnitudes can be recovered, the magnitudes of the second band are prone to significant errors for bright stars. Because of this, we do not trust the 4.6μm measurements for magnitudes smaller than ~6 (in our case, absolute magnitudes smaller than ~8-9), which means large parts of our stellar sample. We illustrate this in Figure 1. Because of this, we focus on the 12 and 22 μm bands as well as the 3.4 μm band.

### 2.2.1. WISE data quality

The *WISE* survey gives, in addition to the magnitudes in the four bands, error estimates for these four magnitudes. In order to check both the data as well as the error estimates, we compare

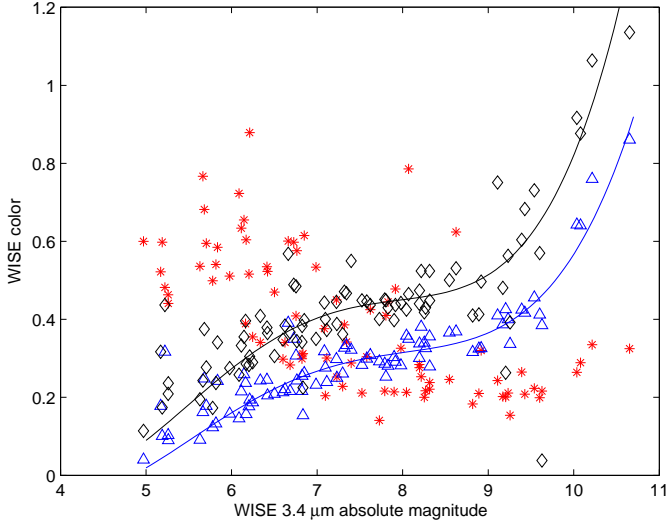


**Fig. 1.** WISE [3.4]-[4.6] color (red stars), [3.4]-[12] color (black diamonds) and [3.4]-[22] color (blue triangles), plotted against the 3.4  $\mu\text{m}$  absolute magnitude. Both the [3.4]-[12] and the [3.4]-[22] color show the expected trend (they get more red for late-type stars) and can be fitted with a polynomial. The [3.4]-[4.6] color is expected to show a similar trend and furthermore be smaller than the other two colors for any spectral type. This is clearly not the case for the bright end of our sample (above magnitudes of  $\sim 6$  or absolute magnitudes of  $\sim 8-9$ ). We therefore omit the second channel in our analysis.

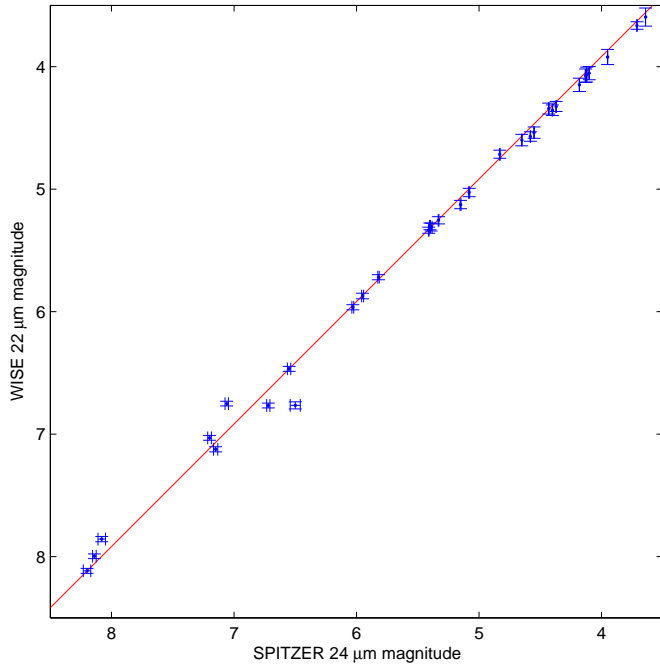


**Fig. 2.** Comparison of WISE and *Spitzer* data for the sources in common with Gautier et al. (2007). The red line shows a weighted least-squares fit for the offset between the *Spitzer* and WISE magnitudes, which is 0.083 mag with the WISE magnitudes being fainter. This offset exists due to the different wavelength passbands (centered at 22  $\mu\text{m}$  vs. 24  $\mu\text{m}$ ). The WISE data match the *Spitzer* data very well with only a few outliers at the faint end.

the w4 (22  $\mu\text{m}$ ) band data with data from Gautier et al. (2007), who did a similar study using observations with the *Spitzer* space telescope. Some of our samples overlap (the corresponding stars are marked with  $^{\circ}$  in Table 2). *Spitzer*, providing pointed observations, performs significantly better than WISE in measuring infrared magnitudes. For the 34 stars where both *Spitzer* 24  $\mu\text{m}$  and WISE 22  $\mu\text{m}$  data ARE available, the *Spitzer* formal uncertainties (not including systematic calibration uncertainties, c.f. Gautier et al. (2007)) are consistently smaller, often by a factor exceeding 10. We can thus use the *Spitzer* data as a benchmark for the WISE data, as we have done in Figure 2. There is a slight offset between the *Spitzer* and WISE magnitudes which we determine to be 0.083 magnitudes using a weighted least-squares fit. For the high-luminosity end, the fit is very good and suggests that the WISE errors might actually be overestimated (or there is a fraction in these errors which represents the global calibration uncertainty, which has no influence on this comparison other than a global offset, which we correct for). At the low-luminosity end, there are some outliers. At least one of these outliers can be explained because visual inspection shows that the WISE source is not well centered on the actual source. We conclude from this that at least in the longest wave band, the data quality is mostly good, but some outliers might be expected. No such statement can be made about the other wave bands. However, as our analysis will show, the data quality is in fact excellent and the WISE errors seem to be generally overestimated.

### 3. Analysis

For our 85 systems, we have magnitudes in seven different bands (V, the 2MASS bands *J*, *H* and *K<sub>s</sub>*, as well as the WISE bands w1, w3 and w4). In addition, we also have parallax and thus distance information, giving us access to the absolute magnitudes. The difficulty we face with M dwarfs is that, unlike solar-type or A stars, they are not well into their Rayleigh-Jeans tail at 3.4  $\mu\text{m}$ . This means that not only the *J-H*, *J-K<sub>s</sub>* and *H-K<sub>s</sub>* colors depend on spectral type, but that the same applies for the colors in the WISE bands.

#### 3.1. A proxy for stellar temperature

Because we expect the dependence of the WISE colors for stars without excess to be mainly with the effective stellar temperature  $T_{\text{eff}}$ , we need a good proxy for this. Casagrande et al. (2008) have shown that none of the 2MASS colors (*J-H*, *J-K<sub>s</sub>*, *H-K<sub>s</sub>*) are good proxies for effective stellar temperature, but show significant scatter and are not necessarily a monotonic function of spectral type. Good proxies are the *V-K<sub>s</sub>* color as well as absolute magnitudes in a variety of bands.

The spectra of M dwarfs are dominated in the visible TiO bands. The *V* band flux for a given  $T_{\text{eff}}$  may therefore significantly depend on abundances and atmospheric dynamics. Furthermore, many M dwarfs are known to be variable in the visible band (e.g., Hawley (1993)), which in turn can influence the *V-K<sub>s</sub>* color, depending on at which point in the variability cycle the *V* band data was taken. To assess this, we plot the absolute 3.4  $\mu\text{m}$  magnitude obtained from WISE against the *V-K<sub>s</sub>* color in Figure 3. If indeed both are good proxies for stellar temperature, we expect to be able to fit a (not necessarily straight) line through the data points. This is clearly not the case. Plots against the *K<sub>s</sub>* and *V* absolute magnitude show that the main contribution to the scatter comes from the *V* magnitude.

We conclude that because of strong molecular absorptions and variability in the *V* band, the *V-K<sub>s</sub>* color is not an ideal proxy

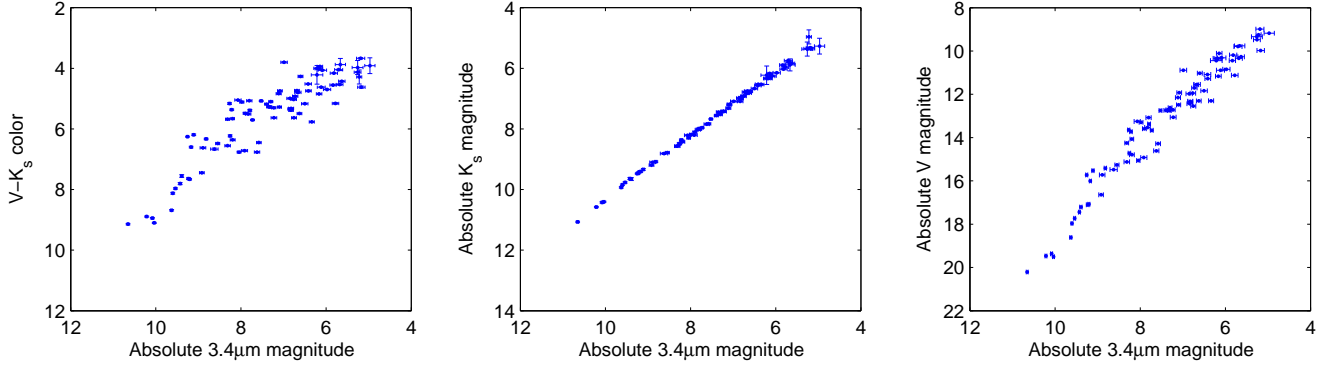


**Fig. 3.** Comparison of WISE absolute magnitudes in w1 ( $3.4\ \mu\text{m}$ ) band with  $V-K_s$  color (left panel). As can be seen, the two proxies for stellar temperature do not match well. This is not because of the  $K_s$  magnitude (as can be seen in the middle panel), but because of the magnitude in the visual band (right panel). An empirical determination of M dwarf mid-infrared colors as a function of the  $V-K_s$  color index can be found in the appendix.

for stellar temperature for late-type dwarfs. We choose to use the  $3.4\ \mu\text{m}$  absolute magnitude instead, because it is a good proxy for stellar temperature and furthermore can give us the best data consistency because it originates from the same instrument. The reduced  $\chi^2$  goodness-of-fit measurements of our analysis support this choice because the fits to the data are better.

There is one caveat to using absolute magnitudes as a proxy, though. Because pre-main-sequence stars are too bright for their spectral type due to their larger diameters, the predictions for their spectral types / surface temperatures and thus their colors in the mid-infrared will be off (c.f. Section 3.8). For this paper, this is not an issue because there are no known pre-main-sequence stars in our sample. For young stars, however, it is better to use the  $V-K_s$  color as a proxy, which is indeed also a very decent proxy for stellar temperature even for these late-type dwarfs. We show the fit against the  $V-K_s$  color index for comparison and reference in the appendix.

### 3.2. Variability in the WISE bands

As we have discussed above, many M dwarfs are known to be variable in the visible. Several of our stars are flare stars, producing short-term variability in the ultraviolet. Out of the 34 stars in our sample that were also observed with *Spitzer* by Gautier et al. (2007), the SIMBAD database marks more than half as flare and/or variable stars. While we cannot comment on the accuracy of these classifications, we see that flare and variable stars are part of this sample. On the other hand, we see that the *WISE* and *Spitzer* magnitudes match well (cf. Figure 2) at the bright end, while outliers are present at the faint end. Tofflemire et al. (2012) observed three M dwarfs for flares and short-term variability and found that while the flares are intense in the ultraviolet, the variability they produce in the near-infrared 2MASS regime is below 7-11 mmag depending on the band. From this we conclude that the outliers in the longer *WISE* bands are mostly not due to variability, but have other reasons (for example, bad centering, background contaminations or contaminations from nearby sources).

We can get rid of most of the variability in the mid-infrared by using the *WISE* colors. All four *WISE* bands are taken at the same time, which means that any variability that influences all mid-infrared bands equally will not influence the *WISE* colors at all. The *WISE* catalog provides a variability flag for each of the four bands. Out of the 85 sources in our sample, only a small

minority of seven are flagged as variable in at least one of the bands. We conclude that variability is likely to not be an issue for excess detection in our analysis for most of our sample.

### 3.3. Multiplicity

As we have noted before, *WISE* is not able to resolve all known multiple systems within our sample. Because we do not want to exclude these systems from our study, we have to investigate what happens to the *WISE* magnitudes and colors in multiple systems.

Equal-mass binaries will simply have double the luminosity of the single star, the colors should not be influenced. They move to the left by 0.75 magnitudes in Figure 4. Binaries of different mass will move less in absolute magnitude (compared to their primary alone), but might move slightly upwards if the secondary contributes significantly and has a significantly different color. This effect gets smaller for a larger difference in spectral class and thus a larger color difference because the secondary will then only have a fraction of the brightness of the primary, and we expect these binaries to lie relatively close to the position their primary would occupy in the diagram. The same is in principle true for triple systems, even though somewhat larger deviations are to be expected.

Because of the above discussion, we do not use the multiple systems within our sample to obtain the polynomial fit. We do compare them to the fit, though - bearing in mind that we will have to treat them specially if any of them turns out to show signs for excess. Binary and triple systems are marked in Figure 4. As we expect, the multiple systems lie preferentially above the fitted polynomial line.

### 3.4. Fitting and intrinsic spread of mid-infrared colors

In order to be able to detect excesses, we need to know the expected mid-infrared color for every source. Instead of using model stellar atmospheres, we choose a purely data-driven approach and use the data at hand (which might include excess sources) to fit for the expected mid-infrared colors. This is only possible if the number of data points significantly exceeds the number of parameters to fit. It also assumes that the number of excess sources is small compared to the general sample size, which is a reasonable assumption (c.f. section 4). We use a polynomial of 4th order to describe the mid-infrared colors and ob-

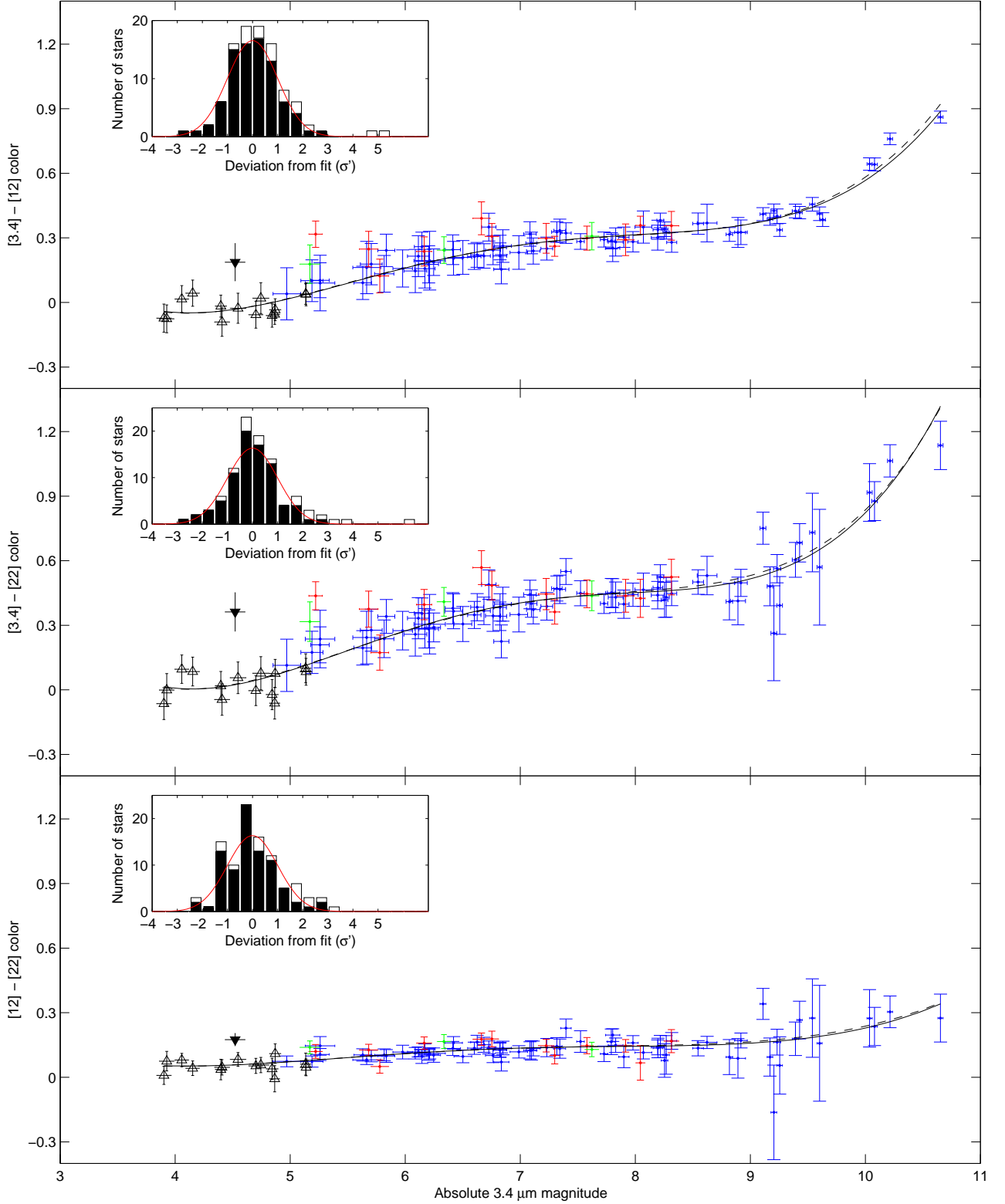


**Fig. 4.** WISE colors plotted against 3.4  $\mu\text{m}$  absolute magnitude. Single M dwarfs are blue, binary systems are marked in red, triple systems in green. The black open triangles show the K dwarfs included to better constrain the high-mass end of the fit. The black dashed line shows the third-order polynomial fit using all single dwarfs, while the black solid line shows the fit after iteratively removing outliers and is used for our analysis. The inset shows the histogram for the  $\sigma'$  error value adopted for our analysis (see definition in the text). The solid bars represent the stars that were used in the fit, the blank stacked bars are for the stars that were omitted in the fit (multiples and outliers). In all three cases, the histograms are consistent with a standard-normal distribution (plotted here as a red line). For reference and as test of our technique, the black filled downward triangle to the left represents the well-known excess source AU Mic, which seems to have significant excess in all three colors. For a discussion of AU Mic, see Section 3.8.



**Table 3.** Statistical tests for  $\sigma'$ 

Color index	KS test (p value)	SW test (p value)
[3.4]-[12]	0.84	0.82
[3.4]-[22]	0.74	0.71
[12]-[22]	0.47	0.41

**Notes.** Probability of the data ( $\sigma'$ ) being drawn from a Gaussian distribution as calculated using the KS (Kolmogorov-Smirnov) and SW (Shapiro-Wilk) tests. All data are consistent with being standard-normal distributed.

tain the fit through an iterative fitting routine which removes outliers in each step (details on this fitting routine and its parameters can be found in the appendix). Outliers are defined as sources that diverge from the fit by more than  $3\sigma'$ .  $\sigma'$  is defined from the data and the fit as:

$$\sigma'_i = \frac{e_i}{\sigma_i} \frac{1}{\sqrt{\chi^2}}$$

Where  $\sigma_i$  is the *WISE* error estimate for source  $i$ ,  $e_i$  is the deviation from the fit and  $\chi^2$  is the overall goodness-of-fit measure of the fit. We note at this point that the iterative fitting procedure does not change the number of excess detections (i.e. there is no excess source which would not have been detected as excess source had we not used an iterative fit).

Gautier et al. (2007) state that the limits for detecting mid-infrared excesses stem from the scatter in photospheric flux predictions from shorter wavelengths and that the mid-infrared properties of M dwarfs are not well known. While we do not predict the mid-infrared fluxes, but instead directly fit the colors, we are also affected by a possible intrinsic spread in the mid-infrared colors, the amount of which is unknown. However, we know that if the intrinsic spread was negligible, our model was a reasonably good fit to the data (which visually seems the case) and the *WISE* error estimates were exactly right, then the deviations from the fit divided by their respective *WISE* error estimates ( $\frac{e_i}{\sigma_i}$ ) should follow a standard-normal distribution and the  $\chi^2$  measure should be  $\sim 1$ . In fact, the  $\chi^2$  measures we obtain are significantly smaller than one, which means that the intrinsic spread must be significantly smaller than the *WISE* error estimates, and furthermore, the *WISE* errors are presumably overestimated.

Because disentangling the errors from the (overestimated) *WISE* measurements and the intrinsic spread would only be possible with a large set of (not necessarily justified) assumptions, we use the above-defined  $\sigma'$  value instead. If the amount of overestimation is about the same for all *WISE* error estimates and if the intrinsic spread is in fact much smaller than these estimates,  $\sigma'$  follows a standard-normal distribution. We present histograms of  $\sigma'$  in Figure 4 as insets. We also use the Kolmogorov-Smirnov-Test and the Shapiro-Wilk-Test to check whether the distributions are compatible with a Gaussian distribution. The results are shown in Table 3. For all three examined colors, there are no hints that the distribution is not Gaussian.

It is worth noting that we fit the three colors individually rather than simultaneously, which means that they are not self-consistent and the net color ( $[3]-[12] + [12]-[22] - [3]-[22]$ ) is not zero. The residuals, however, are so small (0.005 magnitudes on average) that this has no influence on our excess detection technique.

### 3.5. Excess detection

Because of the Gaussian nature of  $\sigma'$ , it can directly be used as a measure to detect excess. We consider a source to show statistically significant excess if  $\sigma'_i > 3$ . First, it is worth to note that no source in any of the three colors shows a statistically significant deficit, defined as  $\sigma'_i < -3$ . This gives us confidence that if we see significant excess, this is not just a statistical outlier.

### 3.6. Excess sources

In our sample, we find two sources with  $\sigma'$  values  $> 3$  in [3.4]-[12] color, three in [3.4]-[22] color and one in [12]-[22] color. We list these sources in Table 4. The six detections are for four individual stars. We discuss each star in detail.

#### 3.6.1. GJ 570 B/C

The binary GJ 570 B/C shows excess at 12 and  $22\mu\text{m}$  and is flagged as variable in all three considered bands. Visual inspection of the *WISE* images shows a second nearby source. The GJ 570 system actually consists of four individual stars: The K4 primary GJ 570 A, the two close M dwarfs GJ 570 B and C, and the T7 brown dwarf GJ 570 D. The brown dwarf is at large separation ( $\sim 250''$ ), the source next to the B/C binary is the A primary at a separation of about  $20''$ . Both sources are bright (3.8 magnitudes in  $K_s$ ), and since they are close, contamination could be an issue. In fact, a close examination of the  $J$ ,  $H$  and  $K_s$  band in combination with the *WISE* bands yields that the GJ 570 B/C is measured more than 0.25 magnitudes less bright in the first *WISE* band than in  $K_s$  and more than 0.3 magnitudes less bright in the first *WISE* band compared to the third. We conclude that the most likely explanation is that the measurement in the first *WISE* band is incorrect. This explains both the apparent excess in the third and in the fourth band, since the colors are calculated against the first *WISE* band. It would not explain any excess in [12]-[22], and indeed no excess is seen at this color (the excess value of  $1.7\sigma'$  is well below our threshold of  $3\sigma'$  and might be artificially enhanced because GJ 570 B/C is a binary, c.f. section 3.3). We therefore conclude that there is no significant sign for excess at either 12 or  $22\mu\text{m}$ .

#### 3.6.2. SCR 1845-6357 A

This single star shows a clear  $4.8\sigma'$  excess at  $12\mu\text{m}$  and no excess at  $22\mu\text{m}$ , although the associated  $\sigma'$  value is 1.9. The derived  $\sigma'$  of 0.87 in [12]-[22] is not significant. It is not flagged as variable in any of the *WISE* bands. The excess in magnitudes over the fitted line is 0.132, 0.144 and 0.064 magnitudes, corresponding to 12.9%, 14.2% and 6.1% excess, respectively, with the caution that the latter two are not significant.

The excess can be explained by the fact that SCR 1845-6357 has a T6 secondary at a separation of  $\sim 1''$  (Biller et al., 2006; Kasper et al., 2007). While T dwarfs usually do not contaminate the flux of a system enough to produce a detectable excess in solar-type stars because of the large difference in emitted flux, SCR 1845-6357 A is a very late M dwarf of spectral class M8.5 (Henry et al., 2006) and thus itself very faint. The T dwarf is fainter by only  $\sim 4$  magnitudes in the  $H$  band (Kasper et al., 2007). While the flux in the  $3.4\mu\text{m}$  band of *WISE* is only on the level of  $\sim 1 - 2\%$  of the M dwarf primary, it can explain the increased flux in the  $12\mu\text{m}$  and  $22\mu\text{m}$  bands. We conclude that the excess is real in both the 12 and  $22\mu\text{m}$  bands, but does likely not originate from a debris disk, but from the T dwarf secondary.



**Table 4.** Sources showing excess in our analysis - discussion in text

Name	[3.4]-[12]	[3.4]-[22]	[12]-[22]	Comment
GJ 570 B/C	<b>5.27</b>	<b>6.05</b>	1.73	Contamination from nearby K4 primary
SCR 1845-6357 A	<b>4.84</b>	1.92	0.87	T6 brown dwarf companion in beam
LHS 288	1.34	<b>3.78</b>	<b>3.49</b>	22 $\mu$ m measurement strongly inconsistent with Spitzer measurement
GJ 860 A/B	2.41	<b>3.21</b>	2.35	Apparent excess caused by binarity

**Notes.** The four sources identified as excess sources from our  $\sigma' > 3$  test with their corresponding  $\sigma'$  values for the three colors we constructed. Statistically significant excesses are marked in bold. The comment gives possible reasons for which the detected excess could be spurious or not originate from a debris disk. The sources are discussed individually in the text.

This shows the validity of our method, which is indeed able to pick up excesses in the 12 $\mu$ m band of as low as 13% for this very late dwarf.

### 3.6.3. LHS 288

LHS 288 is a single star showing excess in [3.4]-[22] (3.8  $\sigma'$ ) and [12]-[22] (3.5  $\sigma'$ ). There is no clear indication that the 22 $\mu$ m measurement of 6.75 magnitudes would be wrong, even though it can be seen in the *WISE* image that there is a diffuse nebulosity in the background. The star is furthermore flagged as variable in the 3.4 and 22  $\mu$ m *WISE* bands. It is worth noting, however, that this source was also measured with *Spitzer* by Gautier et al. (2007). The two measurements are strongly inconsistent, with the *WISE* measurement being 9.5  $\sigma$  above the *Spitzer* measurement at 24 $\mu$ m. We conclude that the most likely explanation for LHS 288 is a bad measurement in the last *WISE* band rather than a real excess.

### 3.6.4. GJ 860 A/B

The close M3/M4 binary GJ 860 shows a derived excess at the longest *WISE* band of 3.2 $\sigma'$ . This corresponds to 0.254 magnitudes or 26.3% excess at this wavelength. At 12 $\mu$ m, the excess is at a 2.6 $\sigma'$  level (corresponding to 0.184 magnitudes / 18.4%), the signal in [12]-[22] color is 2.3 $\sigma'$  corresponding to 0.067 magnitudes or 6.4%. The *WISE* catalog flags this source as variable, but only in the third (12 $\mu$ m) band. The system does lie in a crowded region with possible background cirrus, but it is bright itself (magnitude 4.7 at 3.4 $\mu$ m, magnitude 4.1 at 22 $\mu$ m). Other bright sources are nearby, especially one source that is strong at 22 $\mu$ m but weak at the other wavelengths (in comparison to GJ 860). This source lies approximately 90'' to the southwest. It is unlikely that it strongly affects the *WISE* measurement at this wavelength. Because this is a binary star, special precautions are necessary. The increased luminosity of the total system will move the star to the left in our diagram, and the fact that the later-type member of the system will show a more red [3.4]-[22] color will shift it slightly upwards compared to a single M3 dwarf. Assuming that the M3 dwarf is stronger by a factor of 2 in total luminosity, both effects can be calculated and the position of the M3 dwarf alone in the diagram can be derived. Doing so, we derive new values for  $\sigma'$  of 2.3, 1.7 and 1.9, respectively. None of these are significant, and we therefore do not include this source in our excess sources. An excess might be present at levels below our detection threshold.

### 3.7. Excess detection limits

Due to the fact that we handle each star individually rather than setting a general limit on  $F_{IR}/F_{\star}$ , with  $F_{IR}$  being the detected infrared flux and  $F_{\star}$  the expected stellar flux from our model fit, we do not get a global value of an excess detection limit for all our stars. Rather than that, we are able to detect (3 $\sigma'$  limit) infrared flux excesses down to 10% in some stars while in other stars, even a 30% excess would not be detected due to a larger *WISE* measurement error. Because of this, we have to calculate the excess detection limit for each star individually for each color assessed from its *WISE* error and the  $\chi^2$  value of the corresponding color fit. The typical (median) limits we achieve are on average 14.9% for the [3.4]-[12] excess, 17.9% for the [3.4]-[22] excess and 7.0% for the [12]-[22] excess. The mean values are higher due to a few sources where we achieve rather bad detection limits and measure 15.4%, 20.2% and 10.9%, respectively.

These limits can be converted into limits on the fractional dust luminosity  $L_{IR}/L_{\star}$  if we assume a single dust ring of a given temperature (see Fig. 5). As can be seen, we do not put strong constraints at the fractional dust luminosity for cold dust of temperatures lower than  $\sim 50$ K. Large amounts of cold dust could be present around the M dwarfs we observe to have no significant amount of excess at 12 and 22 $\mu$ m. At our most sensitive point, which is in the interesting (because of its link to terrestrial planet formation zones) 100-300K range, we get 3 $\sigma$  upper limits for  $L_{IR}/L_{\star}$  of nearly  $10^{-4}$  in case of Barnard's star (M3.5, 1.8pc) and nearly  $6 \cdot 10^{-5}$  in case of GJ 526 (M1, 5.4pc). These are in fact fairly typical values for our survey, although it depends a little bit on the spectral type - for the earliest stars in our sample, we can go deeper by a factor of  $\sim 2$ , while for the latest stars we are less deep, again by a factor of  $\sim 2$  (both compared to Barnard's star). This is due to the fact that it becomes more and more easy to detect dust the larger the difference in temperature between the dust and the host star is (Backman & Paresce, 1993). Also because of this, following the discussion in Gautier et al. (2007), we realize that while the limits we obtain for the fractional dust luminosity are less stringent than have been derived for earlier-type stars, this in fact corresponds to more stringent constraints on the dust mass at these temperatures (see discussion in section 4.3).

In most of the cases, the [12]-[22] color is in the most sensitive to dust of these temperatures due to the fact that dust at these temperatures produces no significant excess at 12 $\mu$ m and because our excess limits are the most stringent ones in this color.

### 3.8. AU Mic

Although not in our sample due to its distance, it is interesting to have a look at the most well-known M dwarf with a debris disk,

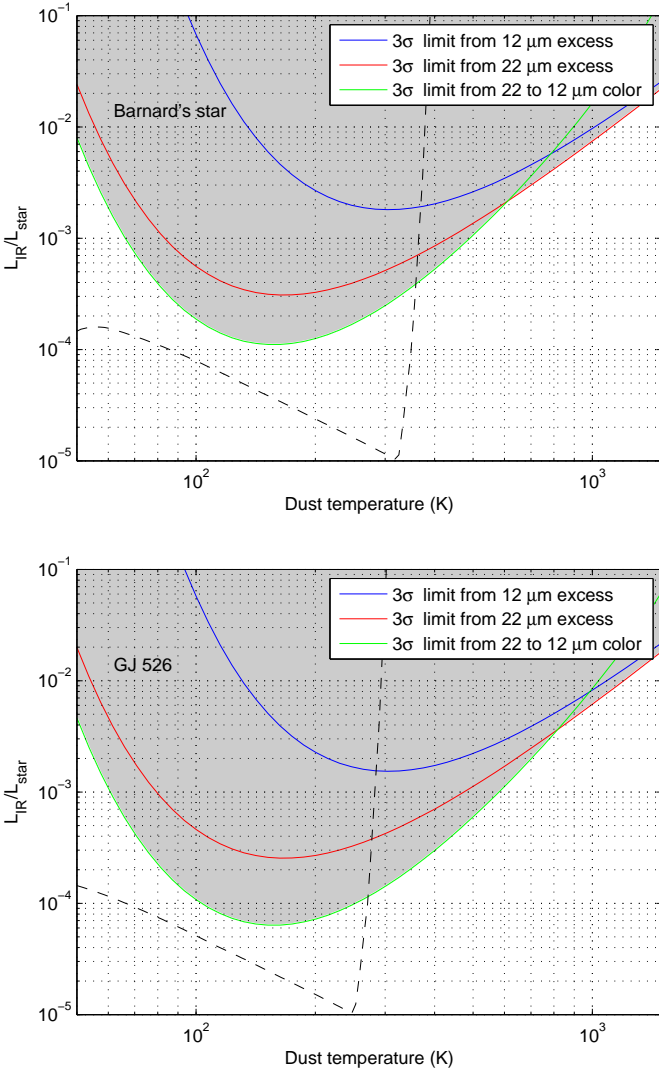


**Fig. 5.** Inferred dust limits for GJ 699 (Barnard’s star, top) and GJ 526 (bottom). The different lines show the limits from the different *WISE* colors. The grey shaded region is excluded by the combination of all three individual limits. For reference, the black dashed line shows the expected performance of SPHERE/ZIMPOL for a thin dust ring (see section 5).

AU Mic, a  $\sim 12$  Myr old M1e star in the  $\beta$  Pictoris moving group (Zuckerman, 2001). While excess emission has been found at wavelengths of  $70\mu\text{m}$  and beyond, no excess has been reported at mid-infrared wavelengths of  $24\mu\text{m}$  or shorter (Liu et al., 2004; Plavchan et al., 2009). We plot it together with the stars from our sample in Figure 4, where it can be seen to have significant excess in all colors ( $3.0\sigma'$ ,  $4.9\sigma'$  and  $5.8\sigma'$ , respectively). However, it lies in the K dwarf regime w.r.t. its absolute  $3.4\mu\text{m}$  magnitude. This is because it has a larger surface area than the average M1 dwarf due to its young age. As we have seen, the M dwarf mid-infrared colors depend on their spectral type / surface temperature, and the absolute  $3.4\mu\text{m}$  magnitude is not a good proxy for either in case of pre-main-sequence stars that are too bright for their spectral type.

It is thus better to use the  $V-K_s$  color as the proxy for stellar temperature for such young stars. Doing so, performing the fits and comparing the colors of AU Mic to them, we obtain  $\sigma'$  values of 0.3, 1.2 and 3.3, respectively, for the  $[3.4]-[12]$ ,  $[3.4]-[22]$

and  $[12]-[22]$  colors. This is significant in the last color, pointing to an excess of  $6.7 \pm 2.0\%$  over the photosphere at  $22\mu\text{m}$ . This can be compared to Plavchan et al. (2009), who did not find a significant excess ( $3.5\%$  above the photosphere,  $1.65\sigma$  using *Spitzer* MIPS) and Simon et al. (2012), who do not detect an excess at  $22\mu\text{m}$  either using the *WISE preliminary release catalog* and a fixed threshold of  $[12]-[22] > 1.0$ , stating that the AU Mic debris disk is too cold for detection with WISE.

This means that no mid-infrared excess is known for AU Mic, but both these results are not inconsistent with its disk having an excess at  $22/24\mu\text{m}$ , albeit a small one. The *Spitzer* MIPS measurement of  $155.2 \pm 3.2$  mJy can be converted to  $4.160 \pm 0.028$  magnitudes using the zero points from the *Spitzer* MIPS Instrument Handbook. This is consistent with the *WISE* measurement of  $4.137 \pm 0.025$  magnitudes, both with and without taking into account the general offset between the *Spitzer* and *WISE* measurements discussed in Section 2.2.1. This means that we only detect the small excess because our method is more sensitive. In fact, comparing the two bands of *WISE* directly using a calibration from other stars might currently be the most sensitive way to detect very small excesses.

Further hints of an excess at smaller wavelengths than previously thought for AU Mic come from an unpublished *Spitzer* IRS high-resolution spectrum of AU Mic ( $5-35\mu\text{m}$ ) taken in 2005. That spectrum has unfortunately never been published, and the data reduction and especially background subtraction is not trivial, but a quick glance at that spectrum does hint at an excess starting at  $\sim 18\mu\text{m}$ . Unfortunately, the IRS spectrum and the MIPS measurement are not compatible, and resolving the apparent contradiction is non-trivial.

There are more caveats to this. Looking at the images in the *WISE* image archive, the centering of the source seems to be not perfect. Because of this, we would be cautious about these measurements of AU Mic. AT Mic, another M4.5 member of the  $\beta$  Pictoris moving group, detected with an excess of  $\sim 15\%$  at  $24\mu\text{m}$  using *Spitzer* (Plavchan et al., 2009), is not detected as having excess using our technique. It is also not perfectly centered in *WISE*. It has an absolute  $3.4\mu\text{m}$  magnitude similar to that of AU Mic, pointing out again that absolute magnitudes are not a good proxy for stellar temperatures / spectral types of pre-main sequence M dwarfs.

#### 4. Comparison to earlier studies

Several studies have been performed on infrared excesses for main-sequence stars. We concentrate here on studies of  $25\mu\text{m}$  and shorter-wavelength excess. The first major survey of this kind was done with IRAS. However, IRAS was largely not sensitive enough for M dwarfs (Backman & Paresce, 1993). Su et al. (2006) searched  $\sim 160$  A stars for excess with *Spitzer*, yielding an excess rate of  $32^{+5}_{-5}\%$ . Moór et al. (2011) concentrate on F-type stars and observed 82 stars with *Spitzer*, out of which 15 show excess at  $24\mu\text{m}$  ( $18^{+5}_{-4}\%$ ), but in this case, the sample selection was biased towards stars that had hints for excess from other surveys. A more recent survey combining *Spitzer* and *WISE* data for a total sample of 263 F stars detects excess in 19 sources, corresponding to  $7.2^{+1.7}_{-1.5}\%$  (Mizusawa et al., 2012, submitted). Trilling et al. (2008) observed nearly 200 sun-like (FGK) stars and found that the incidence of debris disks detectable at  $24\mu\text{m}$  is  $4.2^{+2.0}_{-1.1}\%$ . They also specifically targeted binary and multiple early-type (A3-F8) systems and found that the incidence of debris disks is comparable to or slightly higher than for single stars (Trilling et al., 2007). Carpenter et al. (2009) also target solar-type stars, concentrating on the evolution of detectable excesses

with age. They find that the fraction of systems with detectable excesses ( $> 10.2\%$  above the photosphere) at  $24\mu\text{m}$  drops from  $15^{+3}_{-3}\%$  for ages  $< 300$  Myr to only  $2.7^{+1.9}_{-1.3}\%$  for older ages. Bryden et al. (2009) used *Spitzer* to determine whether the incidence of detectable excesses is different for stars known to harbor planets from radial-velocity searches. They find that any observed difference to stars not known to harbor planets is not statistically significant, but add to the general picture by adding observations of 104 stars of spectral types F through M of which four ( $2.7^{+1.6}_{-1.2}\%$ ) show detectable excesses at  $24\mu\text{m}$ . None of their excess sources is an M dwarf.

All these surveys target stars earlier than spectral type M. Plavchan et al. (2005) pointed out that there is a lack of debris disk detections for mature M dwarfs and discussed possible reasons. Gautier et al. (2007) performed a *Spitzer* search around nearby 62 M dwarfs (some of their targets coincide with the ones in this paper) and found no excesses at  $24\mu\text{m}$ .

The study by Fujiwara et al. (2009) was performed using the data from the all-sky *AKARI* satellite. Their detection threshold is significantly higher at 50% above the photosphere (at  $18\mu\text{m}$ ), where they find significant excess around 14 main-sequence stars and derive an excess fraction of 1.5%. None of their excess stars is a K or M dwarf.

#### 4.1. Dust at similar temperature

As described above, we do not detect a significant excess which holds up to critical assessment in any of our stars. Because we studied 85 targets in the  $3.4$  and  $12\mu\text{m}$  bands and 84 targets in the  $22\mu\text{m}$  band, we derive an excess fraction (at the described levels) of  $0^{+1.3}_{-0.0}\%$  amongst M dwarfs. We do not consider the physically real excess around SCR 1845-6357 A because it stems not from a debris disk, but from a T dwarf binary. T dwarf binaries will not produce detectable amounts of excess around AFGK stars, given current photometric precisions.

The discussion is somewhat complicated by the fact that for some of the targets, we have more than one target in the beam. Considering only targets with single stars in the beam (70 at  $3.4$  and  $12\mu\text{m}$ , 69 at  $22\mu\text{m}$ ) yields an excess fraction of  $0^{+1.6}_{-0.0}\%$ , with some of them being part of wide-separation (distinguishable by *WISE*) binaries. However, Trilling et al. (2007) show that the excess fraction in binary systems is comparable to or slightly higher than the one for single stars for a sample of A and F main-sequence stars. Furthermore, not all studies mentioned above consider only single stars. Because of this, we decide to directly compare our derived excess fraction of  $0^{+1.3}_{-0.0}\%$  to the studies of AFGK and M dwarfs performed in the literature.

Our derived detection rate for M dwarfs is lower than for any other spectral class. This effect can not simply be explained by the fact that our survey is less deep. While we reach only a median excess detection limit of 17.9% in the  $[3.4]-[22]$  color (to be compared with usually  $\sim 10 - 15\%$  for the *Spitzer* surveys), our median excess detection limit in the  $[12]-[22]$  color is 7.0%. In the most sensitive temperature range, the  $[12]-[22]$  color usually gives the strictest limits (c.f. Figure 5). We conclude that we should have been able to detect a comparable percentage of excess systems as what would have been possible with a *Spitzer* survey of the same targets.

Comparing to the A star survey of Su et al. (2006), we can conclude that (randomly selected) M dwarfs have a lower fraction of excess systems at a  $\sim 6\sigma$  level. Comparing to the F star sample of Mizusawa et al. (2012, submitted), the difference of the combined M dwarf surveys is significant on a  $\sim 3.6\sigma$  level. However, as is shown by Carpenter et al. (2009), the fraction of

excess systems is strongly dependent on age. A and F stars are preferentially younger (since they live shorter). Our sample of nearby M dwarfs is likely to be sampled from the average population of M dwarfs in our galaxy, we assume an average age of several Gyr (the star formation rate of the Milky Way peaks at ages  $\sim 2-6$  Gyr, (Wyse, 2009)). The stellar age of the sample from Su et al. (2006) is on average only a few hundred Myr, with no star older than 1 Gyr. Mizusawa et al. (2012) do not have exact ages but estimate that their sample is probably on average  $\sim 300$  Myr. Carpenter et al. (2009) find that the excess fraction for FGK stars drops to 3.6% for ages 300-1000 Myr and 1.8% for ages  $\geq 1000$  Myr. They also find that the upper envelope for  $24\mu\text{m}$  excess at ages  $\geq 500$  Myr is  $\sim 10\%$ . If the same was true for our M dwarf sample, of which the vast majority is expected to be older than 300 Myr and a majority to be older than 1000 Myr, this means three things: 1) The declining excess fraction with age can explain the scarcity of M dwarf excess detections at  $24\mu\text{m}$  and shorter wavelengths, 2) The excess fraction of M dwarfs is not, on a  $3\sigma$  level, statistically different from the excess fraction of FGK stars, and 3) We might be missing some debris disks very close to our detection threshold.

Our results are in agreement with Gautier et al. (2007), who did not find any excess around M dwarfs. When combining the two samples for a total number of 112 M dwarfs probed for excess at either 22 or  $24\mu\text{m}$  and making the conservative assumption that 25% of these M dwarfs are in the 300-1000 Myr age range and the rest is  $> 1000$  Myr old, the excess fraction of the M dwarf sample is different from the FGK sample on a  $\sim 1.1\sigma$  level, there is no clear evidence for a fundamentally different excess behavior of M dwarfs at these wavelengths (corresponding to warm dust), but due to the general scarcity of M dwarf excesses, more data is needed to clarify this question.

#### 4.2. Dust at similar radii

In the last section, we have been comparing our  $22\mu\text{m}$  (non)detections for M dwarfs with studies of earlier-type stars at  $24\mu\text{m}$ . This means, however, that we are comparing dust at very different radii. The orbital radius of dust of a given temperature, assuming blackbody grains, scales as  $R_{\text{dust}} \sim L^{1/2}$ . This means that while we are probing dust at scales  $\ll 1$  AU for our M dwarf sample, the same wavelength corresponds to dust at  $\sim 1$  AU for solar type stars and  $> 1$  AU for A stars.

The discussion is further complicated by the fact that the dust behaves distinctly different from blackbody grains. For M dwarfs, blowout due to radiation pressure is not relevant due to their low luminosities. This means that the dominant grain removal processes will be Poynting-Robertson (P-R) and stellar wind drag (Plavchan et al., 2005; Saija et al., 2003). Depending on the stellar wind from the M dwarfs, the stellar wind drag can dominate. Since the stellar winds of M dwarfs are not well known, their effects are difficult to quantify (Plavchan et al., 2005) and the expected grain size distribution around M dwarfs is unknown. On the other hand, grains smaller than the peak wavelength of their thermal emission will not behave like blackbody grains, but instead have higher effective temperatures than blackbody grains at the same location around the star. This means that we are in fact probing orbital radii larger than expected for blackbody grains with our observations (but likely still significantly smaller than the orbital radii we probe with observations at the same wavelengths around earlier-type stars).

Excess emission around stars of any type becomes more rare for shorter wavelengths. Excess at wavelengths shorter than  $22\mu\text{m}$  around main-sequence FGK stars is very rare (see e.g.

Carpenter et al. (2009)). Since dust at similar radii would emit at shorter wavelengths for earlier-type stars, and since we were unable to establish a statistical difference in emission at the same wavelength, we conclude that we cannot establish a statistical difference for dust at similar radii either. We note, however, that the exact behaviour of dust around M dwarfs is complicated and potentially different from the evolution around earlier-type stars, and that a detailed analysis would require modeling the dust population.

Some detections of very hot dust very close to the star emitting in the  $K_s$  band have been made through interferometry (e.g. Absil et al. (2009); di Folco et al. (2007)). However, this dust is close to the sublimation limit and might represent a very different dust population than what we probe with our study.

#### 4.3. Mass limits

The mass limit for the dust is coupled to both the total fractional excess (together with the albedo, this can be converted into the total optical depth around the star) as well as the distance from the star. The closer the dust is to the star, the lower the total dust mass.

As pointed out above, the exact location of the dust is difficult to calculate. However, we note that in general, we are more sensitive to small amounts of dust than comparable studies for earlier-type stars. Gautier et al. (2007) point out that their 24  $\mu\text{m}$  observations of comparable depth lead to upper limits for the dust mass as low as  $10^{-9}M_{\oplus}$ , although they do not state their assumptions. Because the location of blackbody dust grains scales as  $R_{\text{dust}} \sim L_{\star}^{1/2}$ , the dust mass detection limit scales as  $M_{\text{dust}} \sim L_{\star}$ , so the main reason we are able to place very strict limits on the dust masses is the low luminosities of the M dwarfs.

Assuming blackbody grains of Bond albedo 0.3 and a single grain size of 1  $\mu\text{m}$  with a density of 2.5  $\text{g}/\text{cm}^3$ , we arrive at upper limits for the dust mass ( $3\sigma$ ) of  $1.7 \times 10^{-9}M_{\oplus}$  for the 0.0035  $L_{\odot}$  Barnard's star and  $2.5 \times 10^{-9}M_{\oplus}$  for the 0.011  $L_{\odot}$  star GJ 526 for dust of  $\sim 150\text{K}$ , and even stricter limits for dust at higher temperatures. We cannot make statements about dust at low temperatures, large amounts of which could be hidden from our survey at larger orbital radii. However, we are not aware of any detections of far-IR or sub-mm excesses for these objects.

## 5. Implications

The dust evolution around M dwarfs is still significantly less constrained than the evolution around earlier-type stars. The evolution of dust might follow a different path due to the lower luminosity combined with the low surface temperatures (and thus peak emission at longer wavelengths, longer than the smallest grain sizes). Blowout seems to be irrelevant for M dwarfs. Theoretical models developed by Plavchan et al. (2005) imply that the fractional infrared luminosity  $L_{\text{IR}}/L_{\star}$  might be independent of age for old M dwarfs and there might be a fractional excess of  $\sim 9 \times 10^{-7}$  for all M dwarfs. It is important to point out that we would not be able to detect such an excess. We furthermore realize that an equal excess for *all* stars in our sample would not be detected at all - because it would be masked by our fitting routine.

Further investigations will be required to understand M dwarf debris disks in more detail. While the *Spitzer* 24  $\mu\text{m}$  channel is not available any longer and it will be quite a while until we can get data from *JWST*, there are other promising techniques available to find debris disks around M dwarfs. For example,

*Herschel* has strong capabilities in the far-infrared, which allows to study the frequency of colder dust. Studies at even longer wavelengths are possible (and have been done) in the sub-mm regime. To get a complete picture of the M dwarf debris disk population, both short- and long-wavelength studies will be required.

There are other interesting techniques on the horizon as well. Up to now, infrared excess studies have always been more sensitive to circumstellar dust than resolved imaging and thus, the amount of debris disks detected by their SED excess emission is much larger than the number of resolved debris disks. With the upcoming next-generation VLT instrument SPHERE and its high-contrast polarimetric imager called ZIMPOL, (Schmid et al., 2006), this could in fact change. Due to the use of the polarimetric differential imaging technique (e.g. Quanz et al. (2011)), combined with an extreme adaptive optics system, ZIMPOL will have a very small inner working angle (IWA) of  $\sim 0.02''$ . Because a dust ring this close to the star only occupies a small area on the sky, the surface brightness is large even when the total luminosity of the disk in scattered light is very low.

Assuming an unfavorable face-on viewing angle, blackbody grains, a thin dust ring compared to detector resolution, a geometric albedo of 0.3 and scattering albedo \* polarization fraction = 0.1, we estimate the performance of SPHERE in detecting such rings. We convert these predictions into detection limits in terms of  $F_{\text{IR}}/F_{\star}$  and plot these limits in figure 5. This makes use of preliminary performance estimates for ZIMPOL (achievable contrast of 7.8 / 8.1 / 9.5 ( $\text{mag}/\text{arcsec}^2 - \text{mag}$ ) at separations of 0.02 / 0.2 / 1  $''$ ). SPHERE is expected to be more sensitive to warm dust than the analysis we present in this paper. The steep cutoff towards higher temperatures arises from the IWA of ZIMPOL. As we discuss in section 4.2, the real dust of a given temperature might be further out than expected from a blackbody grain calculation due to the grain size distribution. Because of this, this might be able to probe warmer dust. Furthermore, this technique should work better (up to higher temperatures) for nearby sources. For example, for Barnard's star at 1.83pc, we can probe warmer dust than for GJ 526 at a distance of 5.41pc. SPHERE will not replace surveys in the mid- and far-infrared to sub-mm, but allow complementary observations of nearby sources, probing them for hot dust at small separations and attempting to resolve the dust spatially. It allows to target individual stars to clarify uncertain detections or systems that are on the edge to having significant excess, like the GJ 860 A/B system discussed in section 3.6.4. It will also be able to study known debris disks like the one of AU Mic or possibly AT Mic.

Together, all these techniques will hopefully enable us to understand not only the M dwarf debris phenomenon, but debris disks in general in a more detailed way, including their frequency, their evolution and their structure.

## 6. Conclusions

We perform a volume-limited search for mid-infrared excesses at 12 and 22  $\mu\text{m}$  using the RECONS database and the results of the 2MASS and WISE all-sky surveys. Our main findings are:

1. It is possible to fit the infrared colors of M dwarfs with a polynomial using either the absolute magnitude in the first WISE band (3.4  $\mu\text{m}$ ) or the  $V-K_s$  error as a proxy for stellar temperature. The resulting fit enables us to search for excesses down to typically 14.9% for the [3.4]-[12] color,

- 17.9% for the [3.4]-[22] color and 7.0% for the [12]-[22] color ( $3\sigma$  median values).
2. The quality of the *WISE* data is excellent. The reduced  $\chi^2$  goodness-of-fit values for the polynomial fits suggest that either the *WISE* errors are overestimated or there is a significant portion from a systematic calibration uncertainty in these errors, which would be corrected for by our fitting routine.
3. No excess from a debris disk is found in any color within our detection limits. One physical excess is detected around SCR 1845-6357 A, but is shown to come from the T6 companion orbiting this late M8.5 dwarf. This proves the validity of our method. We also find a tentative excess around AU Mic at  $22\mu\text{m}$ , but it is not part of our statistical sample.
4. Compared to surveys for earlier-type stars, our derived excess fraction of  $0^{+1.3}_{-0.0}\%$  is lower, but this is probably an age effect. The excess fraction in the mid-infrared (warm debris) is not significantly different from the excess fraction for old FGK dwarfs.
5. Dust evolution around M dwarfs is complicated and comparisons to earlier-type stars at either the same orbital distance of the dust or the same total dust mass are difficult because the primary clearing mechanisms for small dust are different. We note, however, that the limits on the total dust mass that can be derived from our survey are more stringent than the typical limits for earlier-type stars.
6. The upcoming SPHERE/ZIMPOL instrument will search selected targets for reflected light from warm, close-in dust. This technique should be more sensitive for nearby bright stars than either *WISE* or *Spitzer* and could provide a mechanism to probe dust at very small angular separations.

We conclude that *WISE* is a great tool for studying the infrared properties of M dwarfs and stars in general and will in the future provide a great source of information, just like IRAS did almost three decades ago. The detection limits achievable with *WISE* are close to the limits achievable with pointed observations from *Spitzer*.

In general, there is still a severe lack of knowledge about dust around M dwarfs and further investigation is required both theoretically and observationally in order to understand the similarities and differences of debris dust evolution between M dwarfs and earlier-type stars. While instruments like Herschel can help us to learn more about dust at far-infrared wavelengths, *WISE* and SPHERE/ZIMPOL can help by probing M dwarfs for closer-in, warm dust rings.

**Acknowledgements.** This publication makes use of data products from the Two Micron All Sky Survey, which is a joint project of the University of Massachusetts and the Infrared Processing and Analysis Center/California Institute of Technology, funded by the National Aeronautics and Space Administration and the National Science Foundation.

This publication makes use of data products from the Wide-field Infrared Survey Explorer, which is a joint project of the University of California, Los Angeles, and the Jet Propulsion Laboratory/California Institute of Technology, funded by the National Aeronautics and Space Administration.

This research has made use of the SIMBAD database, operated at CDS, Strasbourg, France.

This research has made use of the RECONS database ([www.recons.org](http://www.recons.org)).

We want to thank Jarron Leisenring for his help with the IRS spectrum of AU Mic.

We want to thank our unknown referee for his/her very detailed and very helpful referee report which allowed us to improve the quality of this paper.

## References

Absil, O., Mennesson, B., Le Bouquin, J.-B., et al. 2009, *ApJ*, 704, 150

- Acke, B., Min, M., Dominik, C., et al. 2012, ArXiv e-prints
- Aumann, H. H., Beichman, C. A., Gillett, F. C., et al. 1984, *ApJ*, 278, L23
- Backman, D. E. & Paresce, F. 1993, in *Protostars and Planets III*, ed. E. H. Levy & J. I. Lunine, 1253–1304
- Bastian, N., Covey, K. R., & Meyer, M. R. 2010, *ARA&A*, 48, 339
- Bessell, M. S. 1991, *AJ*, 101, 662
- Billar, B. A., Kasper, M., Close, L. M., Brandner, W., & Kellner, S. 2006, *ApJ*, 641, L141
- Bryden, G., Beichman, C. A., Carpenter, J. M., et al. 2009, *ApJ*, 705, 1226
- Carpenter, J. M., Bouwman, J., Mamajek, E. E., et al. 2009, *ApJS*, 181, 197
- Carpenter, J. M., Mamajek, E. E., Hillenbrand, L. A., & Meyer, M. R. 2006, *ApJ*, 651, L49
- Casagrande, L., Flynn, C., & Bessell, M. 2008, *MNRAS*, 389, 585
- Decin, G., Dominik, C., Waters, L. B. F. M., & Waelkens, C. 2003, *ApJ*, 598, 636
- di Folco, E., Absil, O., Augereau, J.-C., et al. 2007, *A&A*, 475, 243
- Fitzgerald, M. P., Kalas, P. G., Duchêne, G., Pinte, C., & Graham, J. R. 2007, *ApJ*, 670, 536
- Fujiwara, H., Ishihara, D., Kataza, H., et al. 2009, in *Astronomical Society of the Pacific Conference Series*, Vol. 418, AKARI, a Light to Illuminate the Misty Universe, ed. T. Onaka, G. J. White, T. Nakagawa, & I. Yamamura, 109
- Gautier, III, T. N., Rieke, G. H., Stansberry, J., et al. 2007, *ApJ*, 667, 527
- Hawley, S. L. 1993, *PASP*, 105, 955
- Henry, T. J., Jao, W.-C., Subasavage, J. P., et al. 2006, *AJ*, 132, 2360
- Henry, T. J., Subasavage, J. P., Brown, M. A., et al. 2004, *AJ*, 128, 2460
- Jao, W.-C., Henry, T. J., Subasavage, J. P., et al. 2005, *AJ*, 129, 1954
- Kasper, M., Billar, B. A., Burrows, A., et al. 2007, *A&A*, 471, 655
- Kirkpatrick, J. D., Henry, T. J., & Irwin, M. J. 1997, *AJ*, 113, 1421
- Koerner, D. W., Kim, S., Trilling, D. E., et al. 2010, *ApJ*, 710, L26
- Lestrade, J.-F., Wyatt, M. C., Bertoldi, F., Menten, K. M., & Lapaigt, G. 2009, *A&A*, 506, 1455
- Liu, M. C., Matthews, B. C., Williams, J. P., & Kalas, P. G. 2004, *ApJ*, 608, 526
- Moór, A., Pascucci, I., Kóspál, Á., et al. 2011, *ApJS*, 193, 4
- Murakami, H., Baba, H., Barthel, P., et al. 2007, *PASJ*, 59, 369
- Plavchan, P., Jura, M., & Lipsky, S. J. 2005, *ApJ*, 631, 1161
- Plavchan, P., Werner, M. W., Chen, C. H., et al. 2009, *ApJ*, 698, 1068
- Quanz, S. P., Schmid, H. M., Geissler, K., et al. 2011, *ApJ*, 738, 23
- Rebull, L. M., Stapelfeldt, K. R., Werner, M. W., et al. 2008, *ApJ*, 681, 1484
- Reid, I. N., Cruz, K. L., & Allen, P. R. 2007, *AJ*, 133, 2825
- Rhee, J. H., Song, I., Zuckerman, B., & McElwain, M. 2007, *ApJ*, 660, 1556
- Ribas, Á., Merín, B., Ardila, D. R., & Bouy, H. 2012, ArXiv e-prints
- Roelfsema, R., Gisler, D., Pragt, J., et al. 2011, in *Society of Photo-Optical Instrumentation Engineers (SPIE) Conference Series*, Vol. 8151, Society of Photo-Optical Instrumentation Engineers (SPIE) Conference Series
- Saija, R., Iati, M. A., Giusto, A., et al. 2003, *MNRAS*, 341, 1239
- Schmid, H. M., Beuzit, J.-L., Feldt, M., et al. 2006, in *IAU Colloq. 200: Direct Imaging of Exoplanets: Science & Techniques*, ed. C. Aime & F. Vakili, 165–170
- Simon, M., Schlieder, J. E., Constantin, A.-M., & Silverstein, M. 2012, *ApJ*, 751, 114
- Skrutskie, M. F., Cutri, R. M., Stiening, R., et al. 2006, *AJ*, 131, 1163
- Spangler, C., Sargent, A. I., Silverstone, M. D., Becklin, E. E., & Zuckerman, B. 2001, *ApJ*, 555, 932
- Su, K. Y. L., Rieke, G. H., Stansberry, J. A., et al. 2006, *ApJ*, 653, 675
- Tofflemire, B. M., Wisniewski, J. P., Kowalski, A. F., et al. 2012, *AJ*, 143, 12
- Trilling, D. E., Bryden, G., Beichman, C. A., et al. 2008, *ApJ*, 674, 1086
- Trilling, D. E., Stansberry, J. A., Stapelfeldt, K. R., et al. 2007, *ApJ*, 658, 1289
- Uzpen, B., Kobulnicky, H. A., & Kinemuchi, K. 2009, *AJ*, 137, 3329
- Vigan, A., Bonnefoy, M., Chauvin, G., Moutou, C., & Montagnier, G. 2012, *A&A*, 540, A131
- Werner, M. W., Roellig, T. L., Low, F. J., et al. 2004, *ApJS*, 154, 1
- Wright, E. L., Eisenhardt, P. R. M., Mainzer, A. K., et al. 2010, *AJ*, 140, 1868
- Wyse, R. F. G. 2009, in *IAU Symposium*, Vol. 258, IAU Symposium, ed. E. E. Mamajek, D. R. Soderblom, & R. F. G. Wyse, 11–22
- Yoon, J., Peterson, D. M., Kurucz, R. L., & Zagarelio, R. J. 2010, *ApJ*, 708, 71
- Zuckerman, B. 2001, *ARA&A*, 39, 549

## Appendix A: Details on the used fitting routine

For the determination of a fit curve to the color-magnitude data required for the subsequent search for excess sources, we use a polynomial fitting routine. We choose a polynomial degree  $n$  and then proceed as follows:

1. Select only the single stars from the sample of all stars

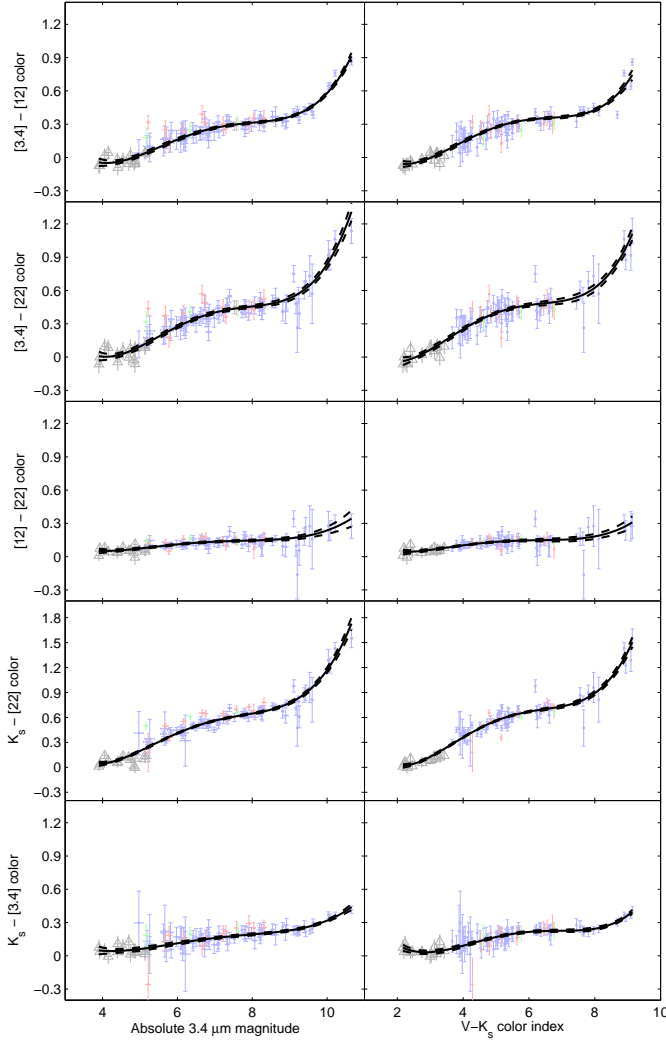


**Fig. A.1.** Obtained fits and error estimates for all three colors and additionally the  $K_s - [22]$  and  $K_s - [3.4]$  colors against absolute magnitude in the first WISE band and against  $V - K_s$  color.

2. Perform a least-squares fit for polynomial of degree  $n$
3. Calculate  $\chi^2$  goodness-of-fit
4. Calculate  $\sigma' = \frac{\sigma}{\sqrt{\chi^2}}$  for all stars
5. Remove stars with  $|\sigma'| > 3$  from the sample
6. Repeat from 2) until converged

We do this for polynomials of increasing degree, starting with  $n = 1$ . We see that for all colors, the quality of the fit does not increase significantly beyond  $n = 4$ , so we choose to use polynomials of fourth degree in all cases.

From the  $\chi^2$  value of the fit, it is possible to estimate the amount of intrinsic scatter in the stellar colors, assuming the error estimates for WISE are correct. As seen before, the WISE errors are likely to be overestimated because the  $\chi^2$  values for all three fits are smaller than one. We conclude that the intrinsic scatter is small and the actual deviations from the fit are dominated by measurement errors. This is true for all WISE colors ([3.4]-[12], [3.4]-[22] and [12]-[22]). The  $K_s - [22]$ , which we also investigate and show here for reference, has a larger  $\chi^2$  value, and intrinsic scatter (induced by scatter in the  $K_s$  color)

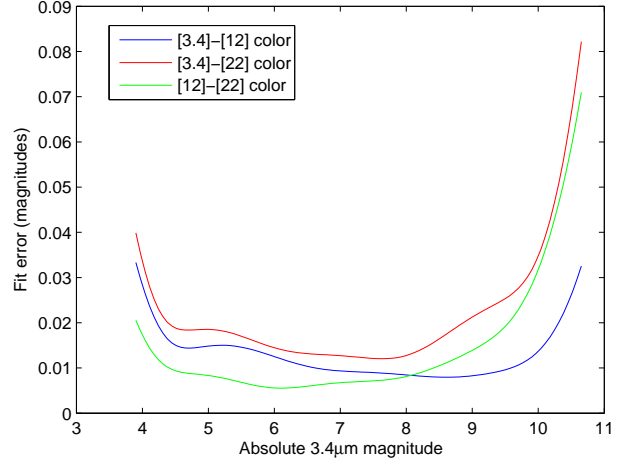


**Fig. A.2.** Inferred errors for our fits. As can be seen, the fit is very well constrained for intermediate M dwarfs, but less constrained at both ends of the fit. At the high-luminosity end, we mitigate this problem through the inclusion of K dwarfs.

might play a more substantial role here.  $K_s - [3.4]$  is very good again, with a low  $\chi^2$  value. We show it here for reference as well as it bridges the *2MASS* longest and *WISE* shortest wavelengths for M dwarfs, which we think could be useful.

While it is possible to obtain uncertainties on the derived parameters of a polynomial fit, this is of limited helpfulness due to the fact that the individual parameters are highly correlated. In order to estimate the error on our fit, we take again a data-driven approach. We use the unmodified  $\sigma$  errors from WISE (not  $\sigma'$ ) and produce 1000 data sets by randomly adding gaussian errors with a standard deviation of  $\sigma_i$  to each measurement. We fit these 1000 data sets using our fitting routine. We can then calculate the uncertainty of our fit at every point by calculating standard deviation of these 1000 obtained polynomial fits.

Figure A.1 summarizes the fits and their upper and lower limits (dashed lines). Because the errors are small and hard to see in this representation, Figure A.2 shows the error of each fit as a function of the absolute magnitude in the first WISE band. As can be seen, the errors are generally small, mostly below 0.02 magnitudes, and thus much smaller than the measurement errors from the individual stars, which is why we do not provide an in-depth discussion of fitting errors in our analysis section (the error is not dominated by the fitting error). At both ends of the fit, the fitting errors naturally get larger, due to the fact that the fit is less constrained at the ends. For the high-luminosity end of the M dwarfs, this effect can be mitigated by including some K dwarfs, as we have done. We have good reasons to believe that our fundamental assumption that the colors can be fitted by a (fourth-order) polynomial holds reasonably well in the stellar regime (namely, the  $\chi^2$  values of our fits are very good).

We summarize the parameters of our obtained fourth-order polynomials in table A.1. The expected color can then be calculated as

$$color(p) = a_0 + a_1p + a_2p^2 + a_3p^3 + a_4p^4$$

with  $p$  being the proxy for the stellar temperature (either absolute  $3.4\mu\text{m}$  magnitude or  $V - K_s$  color). Besides the three WISE bands, we also provide fits for the  $K_s - [22]$  color here. The  $K_s - [22]$  color can also be used for *Spitzer* data using the small offset of 0.083 magnitudes determined in Fig. 2.



**Table A.1.** Polynomial fits

Color	Proxy	$a_0$	$a_1$	$a_2$	$a_3$	$a_4$	$\chi^2$
[3.4] – [12]	$M_{3.4}$	5.6839e+00	-3.9338e+00	9.5780e-01	-9.7494e-02	3.5935e-03	0.6943
[3.4] – [22]	$M_{3.4}$	8.2659e+00	-5.6808e+00	1.3899e+00	-1.4269e-01	5.3063e-03	0.6054
[12] – [22]	$M_{3.4}$	1.7381e+00	-1.1721e+00	2.8991e-01	-3.0074e-02	1.1295e-03	0.5057
$K_s$ – [22]	$M_{3.4}$	6.6826e+00	-4.7923e+00	1.2182e+00	-1.2829e-01	4.8876e-03	1.6584
$K_s$ – [3.4]	$M_{3.4}$	2.2181e+00	-1.4508e+00	3.4410e-01	-3.4285e-02	1.2482e-03	0.5662
[3.4] – [12]	$V-K_s$	5.5283e-01	-7.6010e-01	2.9965e-01	-4.1715e-02	1.9851e-03	1.0173
[3.4] – [22]	$V-K_s$	7.3936e-01	-1.0151e+00	4.2361e-01	-6.2772e-02	3.1802e-03	0.7858
[12] – [22]	$V-K_s$	2.7830e-01	-2.9003e-01	1.1597e-01	-1.7087e-02	8.6622e-04	0.5322
$K_s$ – [22]	$V-K_s$	1.2611e+00	-1.4911e+00	5.8420e-01	-8.3413e-02	4.1207e-03	2.4038
$K_s$ – [3.4]	$V-K_s$	1.2223e+00	-1.1065e+00	3.5304e-01	-4.4812e-02	2.0075e-03	0.4231

**Notes.** Parameters of our estimated polynomial fits for the different colors and the different stellar temperature proxies ( $3.4\mu\text{m}$  absolute magnitude and  $V-K_s$  color). A  $\chi^2$  goodness-of-fit value is given for reference. Description of the parameters in the text.